JACS
JOURNAL OF THE AMERICAN CHEMICAL SOCIETY

Article

pubs.acs.org/JACS

Mechanism of Transient Binding and Release of Substrate Protein during the Allosteric Cycle of the p97 Nanomachine

Sam Tonddast-Navaei and George Stan*

Department of Chemistry, University of Cincinnati, Cincinnati, Ohio 45221, United States

Supporting Information

ABSTRACT: ATPases associated with various cellular activities (AAA+) form a superfamily of ring-shaped motor proteins that utilize cyclical allosteric motions to remodel or translocate substrate proteins (SP) through a narrow central pore. The p97 ATPase is a homohexameric, double-ring member of this superfamily that encloses a central channel with nonuniform width. A narrow compartment is present within the D1 ring and a larger cavity within the D2 ring, separated by a constriction formed by six His amino acids. We use molecular dynamics simulations to probe the interaction between p97 and an extended peptide substrate. Mechanical pulling of the substrate through the p97 pore reveals that smaller work is required for translocation from the D1 toward the D2 compartment than in the opposite direction. These distinct energetic requirements originate in structural aspects and chemical properties of the pore lining. Whereas van der Waals interactions are dominant within the D1 pore, interaction within the D2 pore are strongly electrostatic. Two charged amino acids in the D2 pore, Arg599 and Glu554, provide the largest contribution to the interaction and hinder translocation from the D2 pore. SP threading requires smaller forces when the SP is pulled from the D1 side due to lower barrier to rotation of the His side chains in the direction of the D2 pore. Based on additional simulations of SP binding to two allosteric conformations of p97, we propose that transient binding and release of SP from the pore involves a lever mechanism. Binding to the open pore conformation of p97 occurs primarily at the Arg599 side chain, where the SP backbone is engaged through electrostatic interactions and hydrogen bonds. ATP-driven conformational transitions within the D2 ring alter the chemical environment inside the p97 cavity in the closed pore state. In this state, Glu554 side chains project further into the pore and interacts strongly through van der Waals contacts with the SP backbone. Based on mutations at the two sites in each of the states we identify a specific requirement of these side chains for interaction with the substrate.

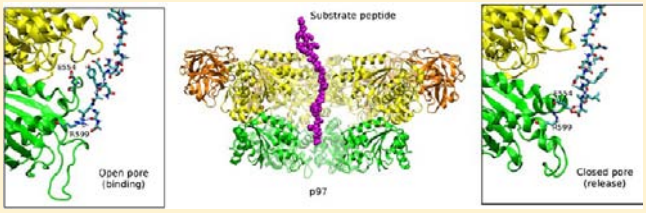

INTRODUCTION

Members of the AAA+ (ATPases associated with diverse cellular activities) superfamily[1,2] are ubiquitous proteins found in prokaryotic cells as well as in multicellular eukaryotes. They participate in a broad range of cellular functions, including DNA replication, membrane fusion, and protein degradation,[3] which renders them essential for cell survival. Most AAA+ proteins effect protein remodeling by promoting protein folding, unfolding and translocation, and assembly and disassembly of complexes. The distinguishing building block of this class is a highly conserved nucleotide binding domain, with ≃200−250 amino acids, known as AAA domain. Subunits containing one (type I) or two (type II) AAA domains assemble into toroidal structures with narrow central channels.

p97 (also called valosin-containing protein or Cdc48) is an eukaryotic type II member of the AAA+ superfamily found abundantly in mammals and yeasts.[4−8] As part of the protein quality control system, it has a critical role in substrate protein (SP) unfolding within the ubiquitin-dependent degradation pathway.[4,9] Each p97 subunit includes two AAA domains, D1 and D2, and the N domain, which is covalently linked to D1 and is involved in interaction with cofactors. The functional structure of p97 is a homohexamer with two stacked rings that comprise the D1 and D2 domains (Figure 1a). Distinct roles of the two rings are indicated by asymmetric structure and catalytic activity.[10−13] The D1 ring encloses a narrow central pore and it is attributed heat-induced activity in ATP hydrolysis,[5] whereas the D2 ring includes a large cavity and it has the major ATPase activity, under physiological conditions, coupled to its greater conformational flexibility.[10,14,15] The two ring compartments are separated by a constriction with diameter ≃4 Å formed by the six His317 side chains. Experimental studies indicating unfolding activity of each of the p97 rings,[16,17] proteolytic activity of the Cdc48·20S complex,[18] and unfoldase action of an archaeal homologue of p97[19] suggest that p97 threads the SP through the His317 gate.

Irrespective of the possible substrate transfer between ring compartments, p97 has been shown to interact with SPs in an ATP-dependent manner.[17,20] A set of amino acids lining the pore in the D2 ring, Trp551, Phe552, Arg586, and Arg599 (Figure 1b), has been identified as critical for this interaction.[17] The two bulky amino acids, Trp551 and Phe552, are part of loops possessing the Gly-aromatic-hydrophobic-Gly motif

Received: April 23, 2013
Published: September 5, 2013

dx.doi.org/10.1021/ja404051b | J. Am. Chem. Soc. 2013, 135, 14627−14636

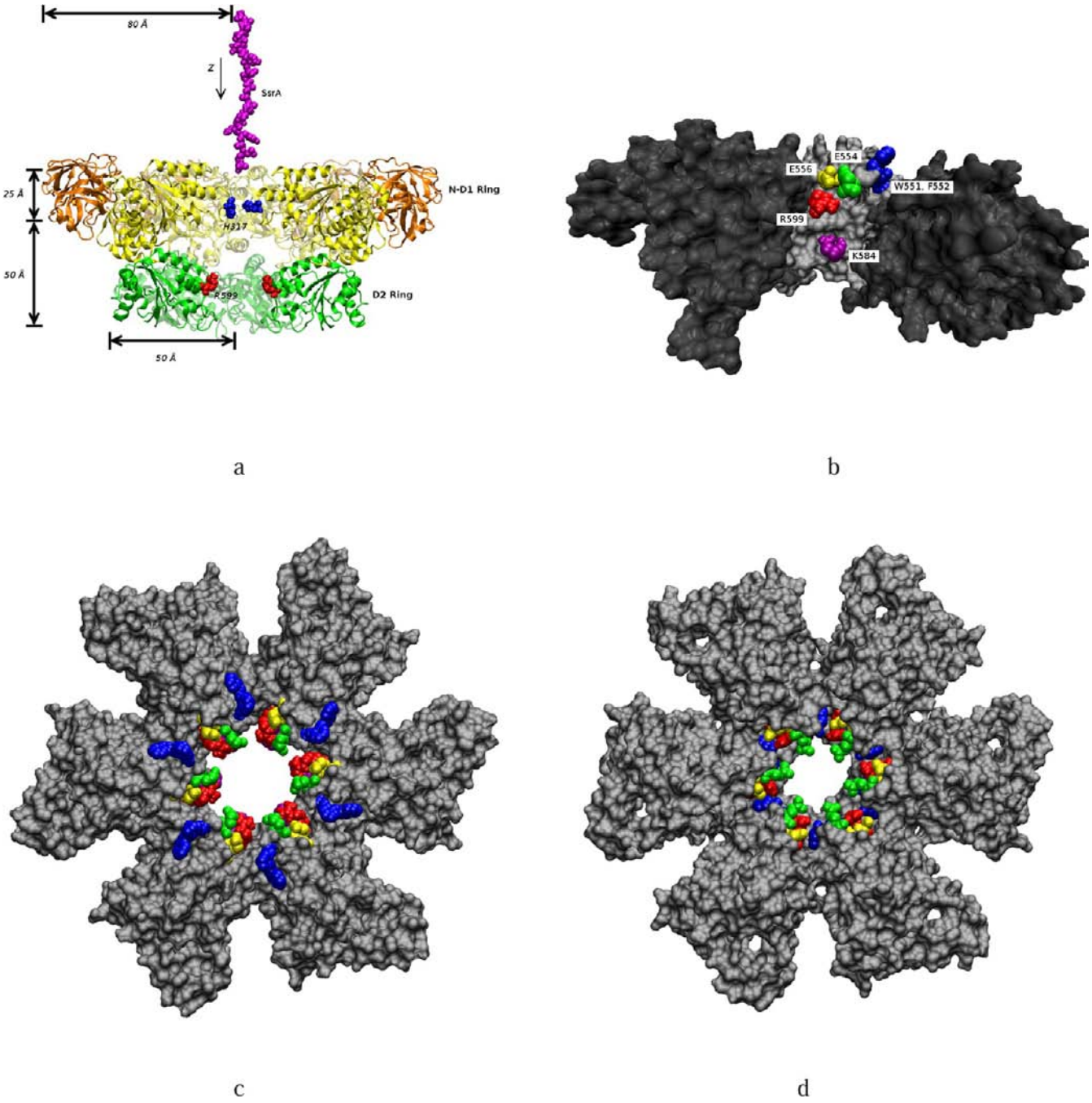

Figure 1. Structural details of p97 and the substrate peptide. (a) Initial configuration of mechanical threading simulations (D1 → D2 is illustrated here). Individual p97 subunits consist of three domains, N (orange), D1 (yellow), and D2 (green). The constriction formed by His317 (blue) amino acids separates the pores of the D1 and D2 rings. Arg599 amino acids (red) are located on the cavity lining of the D2 pore. For clarity, two p97 subunits are not shown. (b) Molecular surface representation of the substrate protein binding region of one subunit (gray) within the D2 pore. The two adjacent subunits (black) are also shown. Amino acids identified as binding sites are indicated by colors and labels. (c-d) Top view of D2 pore (as viewed from the D1 side) in the open (c) and closed (d) state. During the open-closed transition access to the Arg599 site is reduced by the projection of the Glu554 side chain into the D2 channel. Molecular images in this paper are rendered using Visual Molecular Dynamics.[60]

conserved throughout the AAA+ superfamily.[21−23] In *E. coli* Clp ATPases, these loops, which protrude into the central channel and execute large-scale, ATP-driven, conformational transitions, are assigned a dual role in SP recognition and translocation.[21,22,24−26] The recognition mechanism involves a peptide tag, typically SsrA (sequence AANDENYALAA), which is covalently attached to the SP.[27] Translocation is effected by repetitive forces applied by these loops onto the substrate.[22,26,28] Interestingly, in p97, SP binding has been suggested to involve two additional amino acids, Arg586 and Arg599. Conservation of this "arginine collar" in the regulatory particle ATPases of the proteasome[17] suggests an important functional role of these amino acids.

Transient binding and release of SPs, which underlies SP unfolding and translocation in the degradation pathway, represents a fundamental mechanism employed by molecular chaperones to effect protein remodeling. Commonly, this mechanism is illustrated by states that alternate between high

dx.doi.org/10.1021/ja404051b | J. Am. Chem. Soc. 2013, 135, 14627−14636

and low affinity for the SP as a result of ATP-driven conformational transitions. In the protein folding pathway, heat shock proteins (HSPs), such as the GroEL/HSP60 chaperonin or the DnaK/HSP70 chaperone, recruit misfolded SPs in order to prevent harmful aggregation. The recognition process takes place in the high affinity state of the chaperone through exposed moieties that provide favorable interactions. In most cases, the SP binding regions of chaperones comprise primarily hydrophobic amino acids that allow recognition of a broad spectrum of substrates, as shown in the case of the bacterial chaperonin GroEL.[29−32] Nevertheless, specific requirements, such as specialization of binding sites in a multivalent assembly or substrate selectivity, are met by including charged side chains, as noted for the eukaryotic chaperonin containing TCP-1 (CCT).[33−35] In the course of allosteric-driven changes, conformational states with low affinity for SPs are realized by restricting access to the SP binding regions. Dramatic large-scale conformational transitions, which are the hallmark of chaperonin cycles, ensure the switch between the high- and low-affinity states for SPs and promote protein folding.[36,37] Following release from the chaperone binding sites, SPs can experience significantly different chemical environments in the two states. During the GroEL cycle, this corresponds to the switch from predominantly hydrophobic interactions presented by the binding sites to strong electrostatic interactions provided by the cavity lining.[38,39] Interestingly, ATP-dependent processes are not absolutely required for the TBR mechanism. Small HSPs (with monomers of molecular mass between 12 and 40 kDa) which lack nucleotide-binding domains or "minichaperone" fragments comprising the SP binding domain of chaperonins or even chaperonins in the apo state are able to assist folding of SPs with nonstringent requirements.[40−44]

In allosteric cycles of p97, transient binding and release (TBR) of the SP requires finely tuned interactions involving amino acids that line the central pore. Here, we perform molecular dynamics simulations to probe the interaction between the SP and p97. Our results reveal that SP translocation must overcome a larger barrier when the substrate is propagated in the D2 → D1 direction than D1 → D2 owing to the strong interaction with charged amino acids, including Arg599, in the D2 pore. Simulations of SP binding to allosteric states of p97 suggest that TBR involves a lever mechanism that consists in SP binding to Arg599 in the high affinity state and SP release from the active p97 subunit through interaction with the competing site Glu554 (Figure 1c-d).

METHODS

Implicit Solvent Model of p97−SP Interaction. To probe p97−SP interactions in atomistic detail within a computationally accessible time, we use the effective energy function (EEF1)[45−47] implicit solvent model, which combines the CHARMM19 force field[48] with a solvent-exclusion model. The total system size is 35855 atoms, which represent the 3750 amino acids of the p97 homohexamer and the 22 amino acids of the SsrA−SsrA fusion peptide. The end-to-end distance of the fusion peptide, which has a random coil conformation, is 62 Å. Allosteric conformations of p97 are modeled using Protein Data Bank (PDB) structures 3CF1 and 3CF2.[10] The hexameric assemblies of p97 in the two states are built by symmetry operations of the dimer (3CF1) and trimer (3CF2) PDB crystal structures using the PISA software.[49−51] These two structures, which occur during the transition from the ATP-bound state (3CF2) to the ATP† transition state (3CF1), highlight major conformational changes that result from ATP hydrolysis in the p97 cycle.[14] The ATP† → ADP transition involves a root-mean-square-deviation of 0.8 Å between p97 conformations and it is likely to make a small contribution to substrate translocation. According to the narrowest width of the D2 pore, we refer to these conformational states as "closed" (3CF1, with diameter $d \simeq 14$ Å) and "open" (3CF2, $d \simeq 20$ Å). Amino acids in regions 21−269 and 341−469 of p97, which are located in the N and D1 domains and are at least 25 Å away from the pore axis, are constrained to their crystal structure positions. The initial configuration of the missing loop (amino acids 582−597) in the distal region of D2 was modeled in several steps. First, the protein chain was extended at the 582 position by growing the loop residues. The peptide bond between the 597 and 598 positions was satisfied by using energy minimization in vacuum. Harmonic restraints (force constant 1 kcal/(molÅ^2)) were imposed on the heavy atoms of all the amino acids outside the 582−597 region and we applied 50 steps of steepest descent minimization and 400 steps of adapted basis Newton−Raphson method energy minimization in vacuum. In all simulations, the axis of the p97 pore is aligned with the z axis and the p97 center of mass is located at the origin, such that the D2 ring is found on the positive side of the z axis. The CHARMM program[52] is used to perform Langevin dynamics (LD) simulations at $T = 300$ K, using a friction coefficient of 5 ps^{-1} and a time step of 2 fs. Bonds involving hydrogen atoms are constrained to their ideal values using the SHAKE algorithm[53] with an accuracy of 10^{-8}. The four mutants of p97 (Arg599Lys and Arg599Ala in the open state and Arg599Lys and Glu554Ala in the closed state) were model-built, using the CHARMM program, by substituting the side chain at the relevant position within the appropriate PDB structures.

SP Threading through the p97 Pore. In the initial configuration of threading simulations, the SP is aligned with the z-axis such that its C-terminus lies closest to either the D1 ($Z_{initial} = -25$ Å) or the D2 ($Z_{initial} = 50$ Å) pore entrance. We use steered molecular dynamics to mechanically pull the SP with constant velocity through the p97 pore. In these simulations, the force constant is $\kappa = 3.5$ kcal/(mol·Å^2) and the pulling speed is 0.5 or 0.25 Å/ps (Table 1). The pulling force is

Table 1. Simulation Details

name		type	time (ns)	ntraj	$Z_{initial}$[a] (Å)	outcome[b]
constant velocity pulling through the p97 pore[c]	open	D1 → D2[d]	20	24	−25	0.96
		D2 → D1			50	0.17
	closed	D1 → D2	20	24	−25	0.83
		D2 → D1			50	0.42
	open	D1 → D2	10	32	−25	1.00
		D2 → D1			50	0.19
	closed	D1 → D2	10	32	−25	0.97
		D2 → D1			50	0.44
binding in sideD2 pore[e]	open	WT	0.2	40	25	0.74
		Arg599Lys				0.47
		Arg599Ala				0.00
	closed	WT				0.61
		Arg599Lys				0.34
		Glu554Ala				0.73

[a] $Z_{initial} = -25$ Å corresponds to a location closest to the D1 pore entrance, whereas the $Z_{initial} = 50$ Å is closest to the D2 pore. $Z = 25$ Å is the average of axial locations of Arg599 and Arg586. [b] Constant velocity pulling: outcome represents the fraction of trajectories in which the C-terminus of SsrA has passed the His317 ring. Binding simulations: outcome is the average number of hydrogen bonds made by site 599 calculated over the second half of the simulation. [c] Simulations were performed using steered molecular dynamics with pulling speeds of 0.5 Å/ps (10 ns simulations) and 0.25 Å/ps (20 ns simulations). The spring constant is $\kappa = 3.5$ kcal/(mol·Å^2). [d] The arrow indicates that direction of the SP pulling. [e] Initial conformations were obtained using mechanical pulling through D1 pore using a harmonic constraint ($\kappa = 4.0$ kcal/(mol·Å^2) located at $Z = -35$ Å as described in the Methods.

dx.doi.org/10.1021/ja404051b | J. Am. Chem. Soc. 2013, 135, 14627−14636

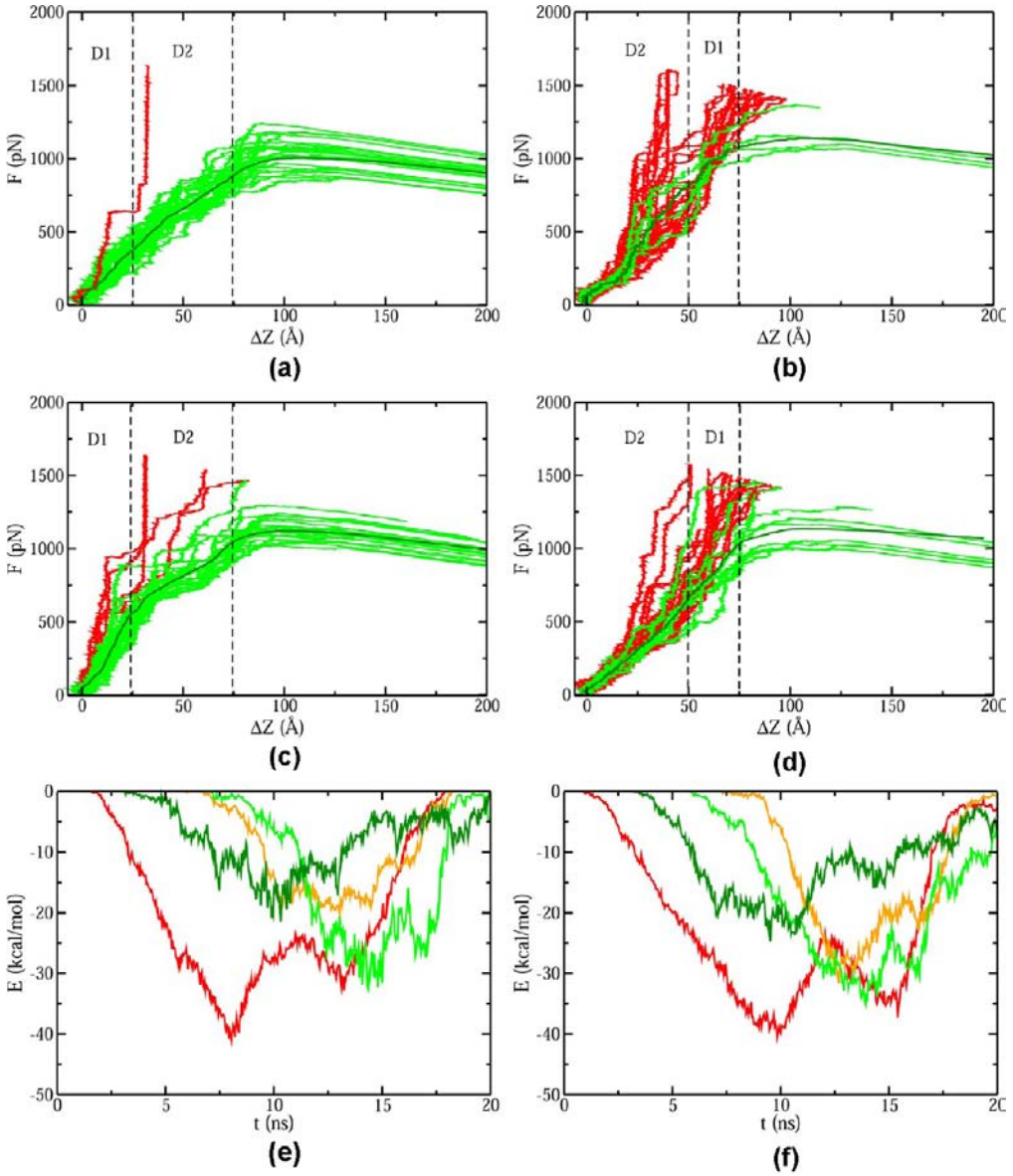

Figure 2. Mechanical threading of the substrate through the p97 pore. (a–d) Force–displacement curves obtained in simulation trajectories of translocation through the p97 pore. Successful translocation (green) corresponds to trajectories in which the C-terminus of the SP passes through the His317 constriction and nontranslocation (red) results in off-pathway trajectories. The average of successful trajectories (dark green) is also shown. (a) D1 → D2 pulling direction in the open state. (b) D2 → D1 pulling direction in the open state. (c) D1 → D2 pulling direction in the closed state. (d) D2 → D1 pulling direction in the closed state. (e, f) Time series of the average interaction energy of the substrate protein with H317 (red for the D1 → D2 direction, green for D2 → D1) and with Arg599 and Glu554 (orange for D1 → D2 direction, dark green for D2 → D1). (e) Open state. (f) Closed state.

applied at the C-terminus of the SP to effect threading in the D1 → D2 or the D2 → D1 direction. Although the duration of each trajectory is significantly faster than the biological time scales of translocation, results of computational studies are relevant as long as the relaxation time scales of the SP, corresponding to binding and unbinding to p97, are much shorter than the pulling time scales. The similar yield of successful translocation events in simulations performed at two pulling speeds (Table 1 and Figure S1, Supporting Information) confirms that the present results are obtained within this regime of validity.

Simulations of SP Binding to Allosteric Conformations of p97. In both open and closed states, the initial configuration of binding simulations is obtained by mechanically threading the SP through the D1 pore and positioning the C-terminus of the SP within the D2 cavity. To achieve this configuration, the SP is aligned with the z-axis such that its C-terminus lies near the D1 pore, at $Z = -35$ Å. A harmonic restraint with force constant $\kappa = 4$ kcal/(mol·Å^2) and origin at $Z = 25$ Å is applied onto the center of mass (CM) of the C-terminus of the SP. The origin of this harmonic constraint corresponds approximately to the midpoint between the centers of Arg599 and Arg586 rings on the pore axis. The restraint is applied during LD simulations at $T = 300$ K for 100 ps. Next, the restraint onto the C-terminus is removed and simulations of SP binding to the D2 pore are performed for 200 ps.

Hydrogen Bond Analysis. In our study, hydrogen bonds are characterized by a distance between donor (D) and acceptor (A) atoms <3.0 Å, the donor–H–acceptor angle >140°, and energy < −2 kcal/mol. The hydrogen bond energy is not an explicit term of the potential energy function in our simulations. The energy of the hydrogen bond is analyzed according to the formula[48]

dx.doi.org/10.1021/ja404051b | J. Am. Chem. Soc. 2013, 135, 14627–14636

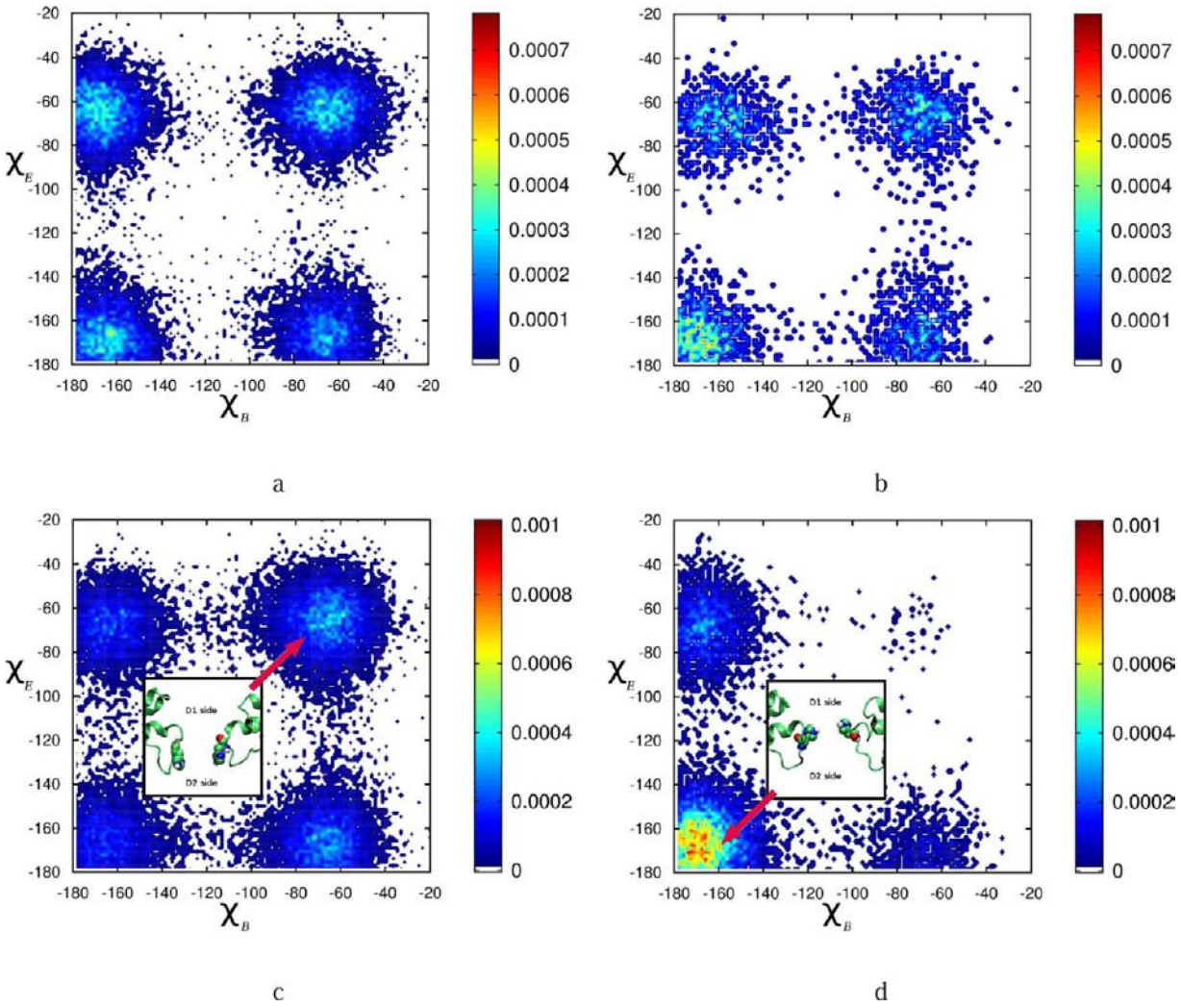

Figure 3. Motions of His317 side chains during mechanical threading of the substrate peptide. Probability density of the χ_1 dihedral angle of His317 side chains in (i,i+3) subunits B and E. (a) D1 → D2 in the open state (b) D2 → D1 in the open state, (c) D1 → D2 in the closed state, (d) D2 → D1 in the closed state. Insets indicate molecular representations of the most populated states.

$$E_{hb} = \left(\frac{A'}{r_{AD}^6} - \frac{B'}{r_{AD}^4}\right)\cos^2(\theta_{A-H-D}) \times f_{sw}(r_{AD}^2, r_{on}^2, r_{off}^2)_{sw}$$
$$[\cos^2(\theta_{A-H-D}), \cos^2(\theta_{on}), \cos^2(\theta_{off})] \quad (1)$$

where r_{AD} is the A−D distance, and θ_{A-H-D} is the A−H−D angle. The switching function, $f_{sw}(x,x_{on},x_{off})$, is 1 for $x \le x_{on}$, $(x_{off} - x)^2$ $(x_{off} + 2x - 3x_{on})/(x_{off} - x_{on})^3$ for $x_{on} < x \le x_{off}$, and 0 for $x > x_{off}$. We chose r_{on} = 2.8 Å, r_{off} = 3.0 Å, θ_{on} = 145°, and θ_{off} = 140°.

The fractional occupancy of hydrogen bonding sites is[54]

$$f_H = \frac{1}{N}\sum_{i=1}^{N}\frac{N_H^{(i)}}{t_i} \quad (2)$$

where $N_H^{(i)}$ is the total number of hydrogen bonds found in the conformations during the trajectory i.

Solvent Accessible Surface Area (SASA) analysis. The solvent accessible area per amino acid is calculated using the Lee and Richards algorithm.[55] The change in SASA of amino acid i of p97, ΔSASA(i), as a result of SP binding, is determined using

$$\Delta SASA(i) = SASA^{p97\cdot SP}(i) - SASA^{p97}(i) \quad (3)$$

where $SASA^{p97\cdot SP}$ is the solvent accessible surface area in the p97·SP complex and $SASA^{p97}$ is the corresponding value in p97 alone.

Interaction Energy Calculations. The interaction energy between amino acid i of p97 with all the amino acids of SP is determined using

$$E_i = \sum_{j=1}^{N_{SP}}(E_{ij}^{(VDW)} + E_{ij}^{(ELEC)}) \quad (4)$$

where the total interaction energy (E_j) is the sum of van der Waals and electrostatic energies between pairs of atoms of the amino acid i of SP and atoms of the N_{SP} amino acids of p97. To calculate the electrostatic interaction, a distance dependent dielectric constant ($\varepsilon_r = r$) is used.[45]

RESULTS

Energetic Requirements for Substrate Translocation through p97. We probed energetic requirements for SP translocation through the central channel of p97 by examining mechanical pulling pathways of the SP, the SsrA−SsrA fusion peptide. To this end, we performed molecular dynamics simulations (see the Methods and Table 1) in which the SP is pulled, with constant velocity, along the central pore of p97, starting from the external opening of either the D1 or the D2 ring (Figure 1a). We considered both open- and closed-pore conformations of p97, which allow us to probe limiting conditions for translocation during sequential conformational

dx.doi.org/10.1021/ja404051b | J. Am. Chem. Soc. 2013, 135, 14627−14636

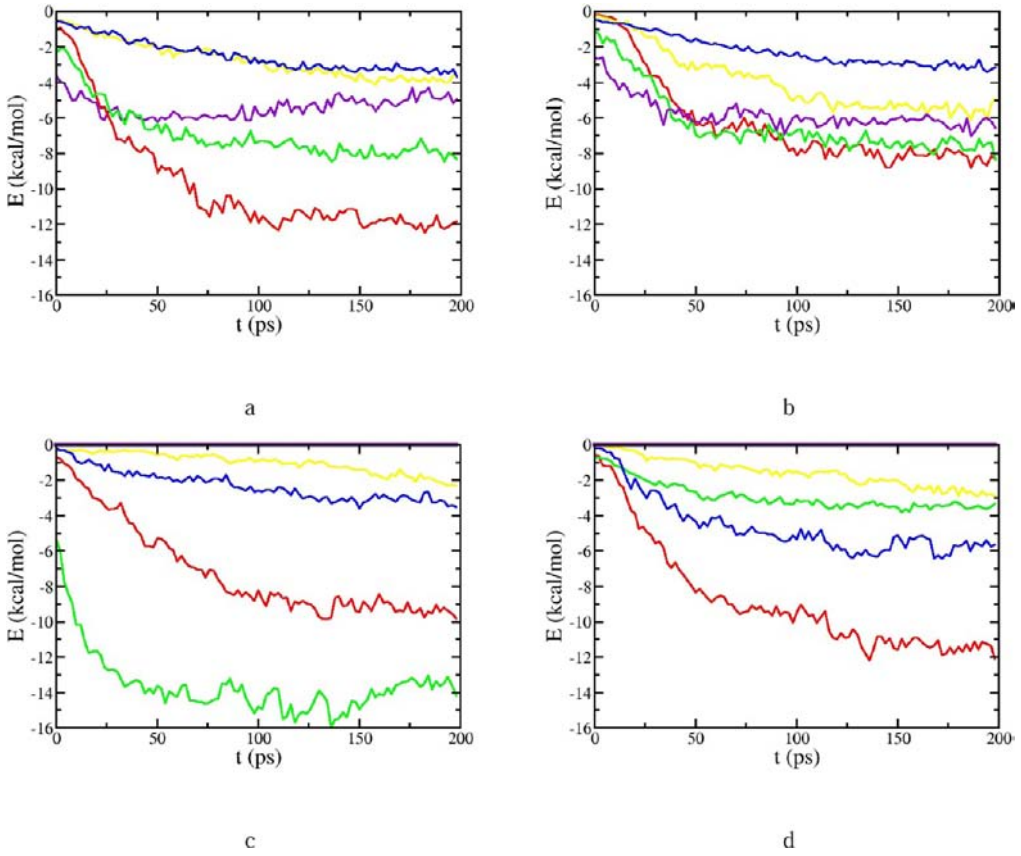

Figure 4. Interaction between the substrate peptide and amino acids in the D2 binding region. Time-series of the interaction energy, averaged over all trajectories, between substrate protein and Arg599(red), Glu554(green), Glu554(yellow), Lys584(purple), and Trp551+Phe552(blue) in the (a) open state, wild-type; (b) open state, Arg599Lys; (c) closed state, wild-type; (d) closed state, Glu554Ala mutant.

transitions of p97 subunits. Independent of the pore width, pulling the SP in the D1 → D2 direction is highly efficient, resulting in complete translocation of the fusion peptide through the p97 pore in nearly all the trajectories (Table 1 and Figures 2a and 2c). By contrast, fewer than 50% of the pulling trajectories in the D2 → D1 direction are successful in threading the SP through the entire pore, even in the closed pore conformation where stronger confinement provides a more favorable environment for translocation. The remaining, off-pathway, trajectories involve deflection of the SP chain off the p97 channel axis and the opening in the His317 diaphragm, which yields divergent pulling forces or unphysical pathways (Figures 2b and d). Consistent with these distinct aspects of mechanical pulling in each direction, force-displacement plots (Figure 2a–d) show that traversing the entrance compartment (D1) in the D1 → D2 translocation requires an average work $\langle W\rangle_{in}^{1\to 2} \simeq 69$ kcal/mol in the open-pore conformation and 101 kcal/mol in the closed-pore conformation, whereas clearing the D2 channel in the D2 → D1 direction requires an average work of $\langle W\rangle_{\mathrm{in}}^{2\to 1} \simeq 296$ kcal/mol (open pore) and 227 kcal/mol (closed pore). In addition, translocation in the D1 → D2 direction requires weaker forces to enlarge the opening of the His317 ring, which has an average width of 7.2 Å in the open pore and 4 Å in the closed pore. As shown in Figure 2a, in most trajectories, a range of forces between 250 and 500 pN (open pore) and 250–600 pN (closed pore) is sufficient in order to increase the width of the His ring-opening to 8.8 ± 1.6 Å. By contrast, when the SP chain is pulled from the D2 side, application of forces between ≃500–950 pN (open pore) and 450–1000 pN (closed pore) results in smaller enlargement of the opening to 7.6 ± 1.4 Å. The D2 compartment is associated with a larger energetic cost for completion of the translocation process. The average work required for exiting the D2 pore in the D1 → D2 direction is $\langle W\rangle_{\mathrm{out}}^{1\to 2} \simeq 460$ kcal/mol (open state) and 579 kcal/mol (closed state), compared to pulling in the opposite direction, which requires $\langle W\rangle_{\mathrm{out}}^{2\to 1} \simeq 342$ kcal/mol (open state) and 297 kcal/mol (closed state) for exiting the D1 compartment. The large work required in the D2 exit compartment suggests that the substrate may partially accumulate within the D2 ring cavity before complete translocation. Overall, these results indicate that mechanical pulling of the SP must overcome energetic barriers related to both the His constriction, at the interface between the p97 rings, and to interactions with the p97 channel lining in each compartment.

To elucidate the microscopic factors that give rise to these barriers, we consider next the detailed interaction of the SP with each of the structural components of p97. In accord with findings outlined above, as shown in Figure S2 (Supporting Information), pulling in the D2 → D1 direction involves a large energetic barrier in the entrance compartment (D2). We find that the strong SP interaction with the D2 cavity lining can be attributed primarily to two sets of amino acids, Arg599 and Glu554 (Figure 1b), which contribute up to ≃−20 kcal/mol (Figure 2e,f). As the SP is threaded into the D1 compartment, the interaction with the His ring involves an additional energy with the minimum value of ≃−35 kcal/mol (Figure 2f). By contrast, pulling in the D1 → D2 direction involves a smaller

dx.doi.org/10.1021/ja404051b | J. Am. Chem. Soc. 2013, 135, 14627–14636

entrance barrier (Figure S2, Supporting Information), while the minimum interaction with the His ring is ≃−40 kcal/mol ((Figure 2c). We note that the larger interaction energy between the SP and the His ring in this pulling direction is due to larger coordination with the six His amino acids. In the D2 → D1 direction, off-axis pathways result in mostly asymmetric interactions with the His ring. In the exit compartment (D2), the interaction with Arg599 and Glu554 amino acids involves a minimum energy of ≃−30 kcal/mol (Figure 2f). Strong contribution of these two amino acids to the SP-p97 interaction, independent of the pulling direction, underscores the importance of these cavity lining sites for the translocation process. To elucidate the distinct interactions with the His ring in the two pulling directions, we monitored the χ_1 (N−C_α-C_β-C_γ) side chain dihedral angle of His317 amino acids. Our results show that the difference in translocation barriers is related to the structural organization of His317 side chains, with more prominent transitions in the closed pore conformation (Figure 3). As shown in the crystal structure of the closed state of p97,[10] the narrow opening of the pore hinders the 6-fold symmetric arrangement of imidazole rings of the His317 amino acids and favors an armchair configuration. In this structure, the χ_1 values of His317 side chains in (i,i+3) subunits are (−85°, −85°), (−128°, −128°), and (−71°, −71°). The pairs of side chains that are close to their gauche(-) orientation (χ_1 = −60°) yield a relatively wider opening of the pore, which is favorable for translocation. By contrast, side chains of the other two subunits, B and E, are closer to their trans (χ_1 = −180°) orientation and must undergo significant motions for pore opening. As shown in Figure 3c, during translocation in the D1 → D2 direction, the most densely populated configurations of His317 side chains in subunits B and E correspond to one or both χ_1 angles in the gauche(−) orientation (−60°). Rotation of the side chain from the reference (crystal structure) orientation, χ_1= −128° to −60°, which represents displacement of the side chain toward the D2 pore, involves a relatively small barrier and a significant widening of the pore. By contrast, as shown in Figure 3d, for translocation in the D2 → D1 direction, the His317 side chain maintain approximately their crystal structure orientation (trans) that corresponds to a closed pore. The large barrier to rotating the His317 side chains toward D1 is overcome, in a fraction of simulations, by in-plane displacement of side chains. Taken together, these aspects explain the lower energetic cost and high efficacy of translocation in the D1 → D2 direction. The analysis of energetic requirements of translocation through the p97 pore indicates that SP threading in the D1 → D2 direction involves lower barriers than in the D2 → D1 direction.

Transient SP Binding to the Open State of the D2 Pore Involves Charged Amino Acids Located on the p97 Cavity Lining. To probe the mechanism of SP binding to the D2 cavity, we perform simulations of the SP confined to the D2 open pore (see the Methods and Table 1). We find that SP binds to a single p97 subunit and it occludes a total solvent accessible surface area (SASA) of ≃246 Å^2 through contacts with several sites (Figure 1d). Two charged amino acids, Glu554 and Arg599, account for most of the total SASA loss (24% and 18% respectively) upon SP binding (Table S1, Supporting Information). Additional important contributions come from the bulky amino acids, Trp551 and Phe552, of the D2 loops (17%) and two charged amino acids, Glu556 (11%) and Lys584 (10%). The remaining contribution (20%) is attributed to binding to Gly533, Ala537, Ala563, Ala577 and Asp578. Examination of the interaction energy between the SP and the binding sites (Figure 4a) reveals that the strongest interaction is at the Arg599 site (average value of −11.6 kcal/mol) and that the SP-Glu554 interaction contributes an additional energy of −8.1 kcal/mol (Table S2, Supporting Information). Other charged amino acids that establish extensive contacts with the SP, Glu556 and Lys584, provide a total energy of −8.9 kcal/mol. Surprisingly, the D2 loop amino acids provide a weaker contribution of ≃−3 kcal/mol to the interaction energy. Overall, these results are consistent with the proposed functional role of central channel loops in gripping the SP and promoting its remodeling in the course of sequential allosteric motions. In addition, our results highlight the specific action of charged amino acids found on the p97 cavity lining. The strong interaction at Arg599 and Glu554, also noted in threading simulations, suggests that these sites are important for transient binding of the substrate during the p97 cycle. We propose that the D2 binding region has a strong charged character, including Arg599, Glu554, Glu556 and Lys584. The weaker interaction at the D2 central channel loops differentiates the p97 action from that of other AAA+ family members, such as ClpY and ClpA, which are suggested to utilize the conserved hydrophobic and aromatic amino acids of the pore loops for both transient SP binding and translocation actions.[21,56]

Binding Mechanism Involves Nonspecific Interactions with the SP Backbone. The charged character of the putative D2 binding region prompts us to examine more closely the p97-SP interactions. We find that the electrostatic interaction represents the dominant term in the binding region, involving primarily the side chains of p97 amino acids and the SsrA−SsrA backbone (Table S2, Supporting Information). At the Arg599 site, the largest contribution (≃69%) to the interaction energy is provided by electrostatic terms. Interaction of the Arg599 side chain with the SsrA−SsrA accounts for 98% of the overall interaction at this site and a large component (≃31%) is provided by the hydrogen bond formed by the Arg599 side chain and carbonyl groups of the SsrA−SsrA backbone. Additional hydrogen bonds with these groups are formed by the Lys584 side chain, while amino acids with opposite polarity, Glu554 and Glu556, interact with the SP primarily through van der Waals interactions. These results suggest that SP binding to the D2 pore takes place through a nonspecific mechanism, which involves handling the substrate chain in a sequence-independent manner.

To probe the specific role of the Arg599 side chain in the hydrogen bond formation and electrostatic interaction, we perform Lys and Ala mutations at this site (Table 1). As shown in Table S2 (Supporting Information), the mutation Arg599Lys preserves the strong electrostatic interaction at this site and the primary role of the 599 side chain in establishing contact with the SsrA−SsrA backbone. Nevertheless, the total interaction energy of Lys599 with the SP is −7.7 kcal/mol (Figure 4b and Table S2, Supporting Information), which is 3.9 kcal/mol weaker than the wild type case (Figure 4a). SP interactions with other charged amino acids are only weakly perturbed (Table S2, Supporting Information). The reduction in interaction strength at the 599 site is nearly completely accounted for by the weaker interaction of the Lys side chain with the SP backbone. The electrostatic and van der Waals terms of this interaction contribute only −5.0 kcal/mol and −1.6 kcal/mol, respectively, to the total energy, compared to ≃ −7.3 kcal/mol

dx.doi.org/10.1021/ja404051b | J. Am. Chem. Soc. 2013, 135, 14627−14636

and −2.3 kcal/mol for the wild type side chain (Table S2, Supporting Information). The weaker interaction of the Lys mutant is attributed, in part, to the shorter side chain, which has a reduced ability to establish contacts with the SP backbone. The shorter side chain effectively increases the width of the pore, which is reflected in the larger initial distance between the SP and Lys and the retardation of the contact formation in the case of the Arg599Lys mutant (Figure 4a,b). The weaker electrostatic interaction of the mutant side chain is reflected in the reduced ability to form hydrogen bonds with the SP backbone (Figure 5a). As shown in Table 1, in the course of

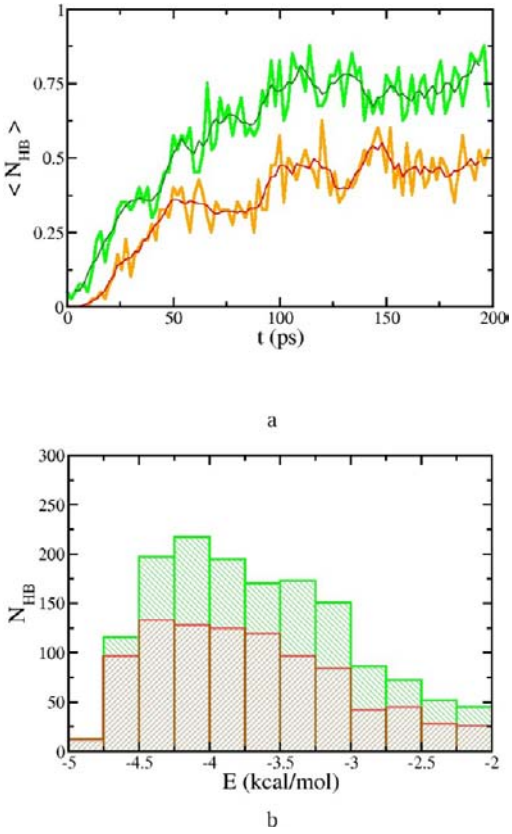

Figure 5. Hydrogen bonds formed by the substrate peptide at the 599 site. (a) Time series of the average number of hydrogen bonds formed with Arg599 (green) and Arg599Lys (red) in the open state. Smooth curves representing running averages are also shown. (b) Histogram of hydrogen bond energies at the 599 site in the wild-type system (green) and Arg599Lys mutant (red).

binding events, the average number of hydrogen bonds of the 599 site is 0.74 for the wild type, whereas for Arg599Lys mutant it is only 0.47. The three donor sites of Lys, compared to four in Arg, yield formation of hydrogen bonds on a slower time scale and with an overall weaker contribution to the interaction energy (Figure 5b).

The Arg599Ala mutation results in a drastic change in the interaction energy between the SsrA−SsrA and site 599 (Table S2, Supporting Information). In this case, the overall interaction energy is −1 kcal/mol and the contribution of the side chain is significantly reduced, whereas SP interactions with other charged amino acids compensate only partially for this change. The weak interaction between the Ala residue and the substrate indicates that this mutation does not preserve the ability to bind the SP at this site. Overall, we surmise that the Arg side chain has a specific role in binding the substrate due to its combined ability to establish van der Waals contacts and hydrogen bonds with the SP backbone. Even a mild mutation, such as Arg599Lys, reduces the strength of the interaction with the substrate and alters the kinetics of contact formation. More drastic changes at this site, such as the Ala mutation, are likely to be deleterious to the binding function. Our results, which are consistent with mutagenesis experiments of central pore residues of p97,[17] provide mechanistic interpretation of the effect of replacing critical side chains lining the D2 pore.

SP Release in the Closed State Involves Lever Mechanism at the Glu554 Site. Efficient substrate propagation during p97 cycles requires the nanomachine to operate by alternating between states with high and low affinity for the SP. The natural states with these distinct characteristics are the open (high affinity) and closed (low) pore states. Topological differences between the allosteric conformations of the D2 ring, revealed by crystal structures, suggest that the Arg599-SP interaction is strongly perturbed in the closed state. Relative motion of Arg599 and Glu554 side chains (Figure 1c,d), which encircle the narrowest region of the D2 pore, result in a reduction of the pore diameter from $d \simeq 20$ Å in the open state to $d \simeq 14$ Å in the closed state. This change in pore width is almost entirely due to motion of Glu554 side chains, as the Arg599 side chains maintain their separation in the two states. To glean factors that underlie the low affinity, we performed simulations of SP binding to the closed D2 pore conformation and compared interactions between the SP and the cavity lining to those in the open state (Table 1). As shown in Table S1 (Supporting Information), we find that SsrA−SsrA binding to the closed conformation results in a significantly smaller occluded surface area of p97 (≃212 Å^2) than in the open state. Consistent with allosterically driven changes in pore geometry, Glu554 provides the dominant contribution, ≃66%, to the total SASA loss of the D2 pore (Table S1, Supporting Information). In the closed state, partial burial of the binding site results in a 55% smaller SASA loss at the Arg599 site and a negligible contribution at the Lys584 and Glu556 sites. Importantly, the D2 pore loop amino acids, Trp551 and Phe552, establish significantly less extensive contacts with the SP in the closed state. Although their SASA is reduced by approximately 15% in the closed state compared to the open state, the SASA loss at these sites is ≃34% smaller (Table S1, Supporting Information). Differences in contact area between the SP and the D2 cavity lining in the two allosteric states are reflected in an overall weaker interaction energy. As shown in Table S3 (Supporting Information), in the closed state, the SP binding energy is ≃8 kcal/mol weaker than in the open state. The contribution of the solvation free energy terms accounts for ≃3 kcal/mol of this difference. Notably, as shown in Figure 4c, in the closed state, SsrA−SsrA interacts more strongly with Glu554 (≃−14.3 kcal/mol) than with Arg599 (≃−9.1 kcal/mol). The weaker interaction with Arg559 in the closed state compared to the open state corresponds to the loss of one hydrogen bond (≃2.5 kcal/mol) at this site, while the interaction with the Glu554 site is strengthened by 6.2 kcal/mol. This switch in interaction strength of the two sites suggests that the allosteric-induced changes in the pore conformation result in SP release from Arg599 through binding at a competing site. We probed this change by performing simulations of the Arg599Lys mutant in the closed state (Table 1). Our results show that the SP−p97 interaction energy of the mutant is weaker by ≃3.5 kcal/mol compared to the wild-type.

dx.doi.org/10.1021/ja404051b | J. Am. Chem. Soc. 2013, 135, 14627−14636

This result is in accord with the smaller exposure of the Lys side chain than Arg and the larger occluding effect of Glu554 on the interaction of the Arg599Lys mutant with the SsrA−SsrA.

At the Glu554 site, the dominant contribution (≃−9.3 kcal/mol) is provided by van der Waals interactions between the side chain and the SP backbone and side chain (Table S2, Supporting Information). The electrostatic term, which involves primarily the Glu554 side chain and the SP backbone, provides an additional ≃−3.4 kcal/mol. Overall, these results indicate that nondirectional interactions involving Glu554 are sufficient to ensure SP release from the Arg599 site while maintaining the grip onto the substrate. To ascertain the specific role of interactions with the Glu554 site in the release mechanism, we also performed simulations of SP binding to closed-pore conformation of the Glu554Ala mutant (Table 1). The mutation effects a large reduction of the interaction between the SsrA−SsrA and the 554 site, from ≃−14.3 kcal/mol in the wild type to ≃−3.4 kcal/mol for the Glu554Ala mutant (Figure 4d). At the same time, the interaction between SsrA−SsrA and Arg599 is effectively restored to its strength in the open state, ≃−11 kcal/mol, and the fraction of hydrogen bonds at the Arg599 site is approximately the same as in the wild-type case (Table 1). Thus, we predict that the shorter side chain at the 554 site is not viable for SP release.

■ DISCUSSION AND CONCLUSIONS

In this paper, we used molecular dynamics simulations to probe energetic requirements of substrate protein translocation through the p97 pore and mechanisms of SP binding and release from p97 subunits during the allosteric cycle. Mechanical threading of the SP through the p97 pore reveals that the translocation in the D1 → D2 direction involves a lower energetic cost than in the D2 → D1 direction. This is primarily due to strong electrostatic interactions of the SP with amino acids that line the D2 cavity, Arg599 and Glu554. This directionality of SP translocation is in accord with recent experiments that indicate the assembly of Cdc48 with the 20S ring into a functional proteasome.[18] In this complex, the D1 ring provides the externally accessible entrance for the SP and the D2 ring, which establishes the interface with the 20S particle, provides the conduit to the degradation chamber. Our results support a translocation model that involves active assistance of Arg599 amino acids in SP threading in the D1 → D2 direction. During sequential intraring conformational transitions of p97, SP binding to Arg599 amino acids of individual subunits provides a mechanical load to promote translocation. Our simulations suggest that this load should be more effective in the initial steps of the hemicycle, when the pore is near its open conformation, but additional translocation assistance can be provided even as the pore closes.

The SP unfolding and translocation action of AAA+ proteins can be formulated as an iterative unfolding mechanism (IUM), by analogy with the iterative annealing mechanism (IAM) framework[57] used to explain the role of TBR in folding assistance. IAM indicates that misfolded conformations are disrupted by promoting the SP onto a higher free energy state and the acquisition of the native conformation is subsequently enabled through kinetic partitioning. In the protein degradation pathway, AAA+ motors must ultimately produce extended SP chains, therefore they disrupt folded structures, which correspond to low free energy states, and favor the unfolded conformations, which have high free energy. Thus, the high affinity state of the AAA+ chaperone must couple to the folded SP conformation and the low affinity state has to favor an extended structure. The potential energy gradient that arises in the alternation between the two states can provide the active force responsible for the unfolding and translocation process. Results obtained in the present study, as well as in previous computer simulations[28] and experiments[58,59] are consistent with these general principles of IUM.

The structural effectors of the active force in AAA domains are the conserved central channel loops. In sequential allosteric transitions, efficient processing of the SP requires that each loop impart force onto the substrate and allow another loop to engage the substrate. The most studied AAA+ motors, the Clp ATPases of *E. coli*, have loops that protrude into the channel and are therefore responsible both for TBR of the SP as well as for the application of force. In this study, we identify a separation of these mechanisms in the p97 machine. Two charged amino acids present on the cavity lining of the D2 pore, Arg599 and Glu554, enable the TBR of the SP through a lever mechanism that switches the predominant interaction from the Arg site in the high affinity state (open pore) to the Glu site in the low affinity state (closed pore). We propose that the functional role of the lever mechanism is to decouple the SP from the force-exerting loop of one subunit, while maintaining it in a competent state for interaction with another active subunit. The central channel loops, which do not provide the largest exposed surface area for the SP in the binding site in either state, are therefore involved primarily in applying the active force onto the SP. This specialization of p97 components for application of force and transient binding-release is likely required to enable functional versatility of this machine.

■ ASSOCIATED CONTENT

Supporting Information

Occluded solvent accessible surface area of D2 binding sites, interaction energies of the SP with charged amino acids on the D2 cavity lining, substrate protein binding energy, translocation results obtained using a pulling speed of 0.5 Å/ps, and time series of interaction energies of the SP with D1 and D2 in threading simulations. This material is available free of charge via the Internet at http://pubs.acs.org/

■ AUTHOR INFORMATION

Corresponding Author

george.stan@uc.edu

Notes

The authors declare no competing financial interest.

■ ACKNOWLEDGMENTS

We gratefully acknowledge insightful comments from Koby Levy and extensive discussions with Sue Wickner and Michael Maurizi. This work has been supported by the National Science Foundation CAREER Grant No. MCB-0952082 to G.S.

■ REFERENCES

(1) Neuwald, A. F.; Aravind, L.; Spouge, J. L.; Koonin, E. V. *Genome Res.* **1999**, *9*, 27−43.
(2) Hanson, P. I.; Whiteheart, S. W. *Nat. Rev. Mol. Cell Biol.* **2005**, *6*, 519−529.
(3) Vale, R. *J. Cell Biol.* **2000**, *150*, F13−F19.
(4) Kobayashi, T.; Tanaka, K.; Inoue, K.; Kakizuka, A. *J. Biol. Chem.* **2002**, *277*, 47358−47365.
(5) Wang, Q.; Song, C.; Yang, X.; Li, C.-C. H. *J. Biol. Chem.* **2003**, *278*, 32784−32793.

(6) Wang, Q.; Song, C.; Li, C.-C. H. *J. Struct. Biol.* **2004**, *146*, 44−57.
(7) Meyer, H.; Bug, M.; Bremer, S. *Nat. Cell Biol.* **2012**, *14*, 117−123.
(8) Chapman, E.; Fry, A. N.; Kang, M. *Mol Biosyst* **2011**, *7*, 700−710.
(9) Beskow, A.; Grimberg, K. B.; Bott, L. C.; Salomons, F. A.; Dantuma, N. P.; Young, P. *J. Mol. Biol.* **2009**, *394*, 732−746.
(10) Davies, J. M.; Brunger, A. T.; Weis, W. I. *Structure (London, England: 1993)* **2008**, *16*, 715−726.
(11) Davies, J. M.; Tsuruta, H.; May, A. P.; Weis, W. I. *Structure (London, England: 1993)* **2005**, *13*, 183−195.
(12) Rouiller, I.; DeLaBarre, B.; May, A. P.; Weis, W. I.; Brunger, A. T.; Milligan, R. A.; Wilson-Kubalek, E. M. *Nat. Struct. Biol.* **2002**, *9*, 950−957.
(13) Zhang, X.; Shaw, A.; Bates, P. A.; Newman, R. H.; Gowen, B.; Orlova, E.; Gorman, M. A.; Kondo, H.; Dokurno, P.; Lally, J.; Leonard, G.; Meyer, H.; van Heel, M.; Freemont, P. S. *Mol. Cell* **2000**, *6*, 1473−1484.
(14) DeLaBarre, B.; Brunger, A. T. *J. Mol. Biol.* **2005**, *347*, 437−452.
(15) Wereszczynski, J.; McCammon, J. A. *Protein Sci.* **2012**, *21*, 475−486.
(16) Rothballer, A.; Tzvetkov, N.; Zwickl, P. *FEBS Lett.* **2007**, *581*, 1197−1201.
(17) DeLaBarre, B.; Christianson, J. C.; Kopito, R. R.; Brunger, A. T. *Mol. Cell* **2006**, *22*, 451−462.
(18) Barthelme, D.; Sauer, R. T. *Science* **2012**, *337*, 843−846.
(19) Gerega, A.; Rockel, B.; Peters, J.; Tamura, T.; Baumeister, W.; Zwickl, P. *J. Biol. Chem.* **2005**, *280*, 42856−42862.
(20) Ye, Y.; Meyer, H. H.; Rapoport, T. A. *Nature* **2001**, *414*, 652−656.
(21) Park, E.; Rho, Y. M.; Koh, O.-j.; Ahn, S. W.; Seong, I. S.; Song, J.-J.; Bang, O.; Seol, J. H.; Wang, J.; Eom, S. H.; Chung, C. H. *J. Biol. Chem.* **2005**, *280*, 22892−22898.
(22) Siddiqui, S. M.; Sauer, R. T.; Baker, T. A. *Gene. Dev* **2004**, *18*, 369−374.
(23) Lum, R.; Tkach, J. M.; Vierling, E.; Glover, J. R. *J. Biol. Chem.* **2004**, *279*, 29139−29146.
(24) Hoskins, J. R.; Singh, S. K.; Maurizi, M. R.; Wickner, S. *Proc. Natl. Acad. Sci. U.S.A.* **2000**, *97*, 8892−8897.
(25) Singh, S.; Grimaud, R.; Hoskins, J.; Wickner, S.; Maurizi, M. *Proc. Natl. Acad. Sci. U.S.A.* **2000**, *97*, 8898−8903.
(26) Hinnerwisch, J.; Fenton, W. A.; Furtak, K. J.; Farr, G. W.; Horwich, A. L. *Cell* **2005**, *121*, 1029−1041.
(27) Flynn, J. M.; Neher, S. B.; Kim, Y.; Sauer, R. T.; Baker, T. A. *Mol. Cell* **2003**, *11*, 671−683.
(28) Kravats, A.; Jayasinghe, M.; Stan, G. *Proc. Natl. Acad. Sci. U.S.A.* **2011**, *108*, 2234−2239.
(29) Kerner, M. J.; Naylor, D. J.; Ishihama, Y.; Maier, T.; Chang, H.; Stines, A. P.; Georgopoulos, C.; Frishman, D.; Hayer-Hartl, M.; Mann, M.; Hartl, F. U. *Cell* **2005**, *122*, 209−220.
(30) Chapman, E.; Farr, G.; Usaite, R.; Furtak, K.; Fenton, W.; Chaudhuri, T.; Hondorp, E.; Matthews, R.; Wolf, S.; Yates, J.; Pypaert, M.; Horwich, A. *Proc. Natl. Acad. Sci. U.S.A.* **2006**, *103*, 15800−15805.
(31) Stan, G.; Brooks, B. R.; Lorimer, G. H.; Thirumalai, D. *Protein Sci.* **2005**, *14*, 193−201.
(32) Azia, A.; Unger, R.; Horovitz, A. *FEBS J.* **2012**, *279*, 543−550.
(33) Jayasinghe, M.; Tewmey, C.; Stan, G. *Proteins* **2010**, *78*, 1254−1265.
(34) Nadler-Holly, M.; Breker, M.; Gruber, R.; Azia, A.; Gymrek, M.; Eisenstein, M.; Willison, K. R.; Schuldiner, M.; Horovitz, A. *Proc. Natl. Acad. Sci. U.S.A.* **2012**, *109*, 18833−18838.
(35) Spiess, C.; Miller, E. J.; McClellan, A. J.; Frydman, J. *Mol. Cell* **2006**, *24*, 25−37.
(36) Yifrach, O.; Horovitz, A. *Proc. Natl. Acad. Sci. U.S.A.* **2000**, *97*, 1521−1524.
(37) Stan, G.; Lorimer, G. H.; Thirumalai, D.; Brooks, B. R. *Proc. Natl. Acad. Sci. U.S.A.* **2007**, *104*, 8803−8808.
(38) Braig, K.; Otwinowski, Z.; Hedge, R.; Boisvert, D. C.; Joachimiak, A.; Horwich, A. L.; Sigler, P. B. *Nature* **1994**, *371*, 578−586.
(39) Xu, Z.; Horwich, A. L.; Sigler, P. B. *Nature* **1997**, *388*, 741−750.
(40) Bepperling, A.; Alte, F.; Kriehuber, T.; Braun, N.; Weinkauf, S.; Groll, M.; Haslbeck, M.; Buchner, J. *Proc. Natl. Acad. Sci. U.S.A.* **2012**, *109*, 20407−20412.
(41) Zahn, R.; Buckle, A. M.; Perrett, S.; Johnson, C. M.; Corrales, F. J.; Golbik, R.; Fersht, A. R. *Proc. Natl. Acad. Sci. U.S.A.* **1996**, *93*, 15024−15029.
(42) Wang, J. D.; Michelitsch, M. D.; Weissman, J. S. *Proc. Natl. Acad. Sci. U.S.A.* **1998**, *95*, 12163−12168.
(43) Stan, G.; Brooks, B. R.; Thirumalai, D. *J. Mol. Biol.* **2005**, *350*, 817−829.
(44) Priya, S.; Sharma, S. K.; Sood, V.; Mattoo, R. U. H.; Finka, A.; Azem, A.; Rios, P. D. L.; Goloubinoff, P. *Proc. Natl. Acad. Sci. U.S.A.* **2013**, *110*, 47199−7204.
(45) Lazaridis, T.; Karplus, M. *Science* **1997**, *278*, 1928−1931.
(46) Lazaridis, T.; Karplus, M. *J. Mol. Biol.* **1999**, *288*, 477−487.
(47) Lazaridis, T.; Karplus, M. *Proteins* **1999**, *35*, 133−152.
(48) Brooks, B. R.; Bruccoleri, R. E.; Olafson, B. D.; States, D. J.; Swaminathan, S.; Karplus, M. *J. Comput. Chem.* **1983**, *4*, 187−217.
(49) Krissinel, E.; Henrick, K. Detection of Protein Assemblies in Crystals. In *Computational Life Sciences*; Berthold, G. R., Diederichs, K., Kohlbacher, O., Fischer, I., Eds.; Springer: Berlin, 2005.; Vol. *3695*.
(50) Krissinel, E.; Henrick, K. *J. Mol. Biol.* **2007**, *372*, 774−797.
(51) Krissinel, E. *J. Comput. Chem.* **2010**, *31*, 133−143.
(52) Brooks, B. R.; Brooks, C. L., III; Mackerell, A. D., Jr.; Nilsson, L.; Petrella, R. J.; Roux, B.; Won, Y.; Archontis, G.; Bartels, C.; Boresch, S.; Caflisch, A.; Caves, L.; Cui, Q.; Dinner, A. R.; Feig, M.; Fischer, S.; Gao, J.; Hodoscek, M.; Im, W.; Kuczera, K.; Lazaridis, T.; Ma, J.; Ovchinnikov, V.; Paci, E.; Pastor, R. W.; Post, C. B.; Pu, J. Z.; Schaefer, M.; Tidor, B.; Venable, R. M.; Woodcock, H. L.; Wu, X.; Yang, W.; York, D. M.; Karplus, M. *J. Comput. Chem.* **2009**, *30*, 1545−1614.
(53) Ryckaert, J.-P.; Ciccotti, G.; Berendsen, H. J. C. *J. Comput. Phys.* **1977**, *23*, 327−341.
(54) Berendsen, H. J. C.; van Gunsteren, W. F.; Zwinderman, H. R. J.; Geurtsen, R. G. *Ann. N.Y. Acad. Sci.* **1986**, *482*, 268−286.
(55) Lee, B.; Richards, F. M. *J. Mol. Biol.* **1971**, *55*, 379−400.
(56) Weber-Ban, E. U.; Reid, B. G.; Miranker, A. D.; Horwich, A. L. *Nature* **1999**, *401*, 90−93.
(57) Todd, M. J.; Lorimer, G. H.; Thirumalai, D. *Proc. Natl. Acad. Sci. U.S.A.* **1996**, *93*, 4030−4035.
(58) Aubin-Tam, M.-E.; Olivares, A. O.; Sauer, R. T.; Baker, T. A.; Lang, M. J. *Cell* **2011**, *145*, 257−267.
(59) Maillard, R. A.; Chistol, G.; Sen, M.; Righini, M.; Tan, J.; Kaiser, C. M.; Hodges, C.; Martin, A.; Bustamante, C. *Cell* **2011**, *145*, 459−469.
(60) Humphrey, W.; Dalke, A.; Schulten, K. *J. Mol. Graphics* **1996**, *14*, 33−38.